Spectroscopy of End-On Copper(II) Superoxido Complexes: A Wave Function-Based Analysis

Léo Chaussy, Vijay Gopal Chilkuri, Stéphane Humbel, Paola Nava

Spectroscopy of End-On Copper(II) Superoxido Complexes: A Wavefunction Based Analysis

Léo Chaussy, Vijay Gopal Chilkuri, Stéphane Humbel, and Paola Nava*

Aix Marseille Univ, CNRS, Centrale Marseille, iSm2, Marseille 13397, France

E-mail: paola.nava@univ-amu.fr

Abstract

Wavefunction methods are employed to analyze the ground and low-lying excited states of bipyramid trigonal copper(II) superoxido complexes, up to their characteristic Ligand to Metal Charge Transfer band. Several multireference methods are combined to provide new insights into the interpretation of their experimental absorption spectra. We show that the intraligand transition on the dioxygen leads to a dark state. Among the results, we shall highlight the finding of doubly excited states in the region of the $d-d$ transitions and the subtle interplay between Cu(I) and Cu(II) in the ground and excited states. Some of these findings could only be obtained with multireference methods.

Introduction

Copper(II) superoxido complexes are at the heart of the activity of several enzymes, and a lot of effort has been devoted to study their properties in synthetic models.[1] We encounter them as key intermediates in several (bio-)chemical processes, such as the oxidation of organic substrates. They are also interesting in the framework of bio-inspired chemistry, as building blocks for developing synthetic catalysts from first-row transition metals, more abundant than their second- and third-row counterparts.[2–10]

Among synthetic copper mono-nuclear superoxido complexes, two kinds of structures have been described: side-on superoxido species have been firstly reported, displaying singlet ground states.[6,11–13] Subsequently, the first X-ray structure of an end-on complex was obtained.[14,15] The end-on $[(L)Cu(O_2)]^+$ complexes have a triplet ground state,[13,16] and they are usually described as copper(II) systems interacting with the radical anion $O_2^{\cdot-}$, $[(L)Cu^{II}(O_2)^{\cdot-}]^+$ (L=ligand, typically TMG3tren=1,1,1-tris[2-[N^2-(1,1,3,3-tetramethylguanidino)]ethyl]amine or TMPA=tris-(2-pyridyl-methyl)amine, Figure 1). Difficult to crystallize, they are characterized in solution by UV-vis spectroscopy at low temperature, as they exhibit an intense LMCT (Ligand to Metal Charge Transfer) at around $\lambda_{max} \approx 430$ nm: several spectroscopic data have been reported on copper(II) superoxido complexes and exhibit similar trends, although absorptions are influenced by the ligand nature and solvent.[8,16–23]

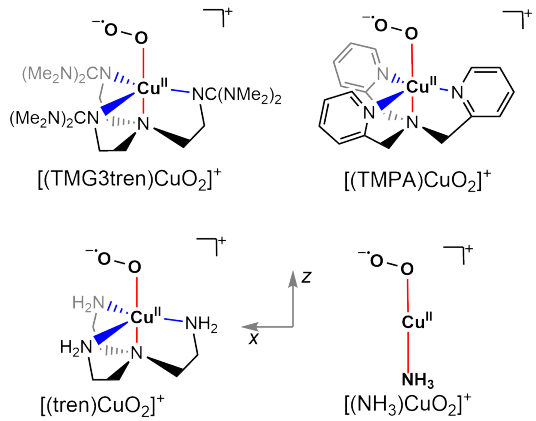

Figure 1: Examples of end-on copper(II) superoxido complexes.

Table 1: Band assignment of $[(TMG_3tren)Cu(O_2)]^+$ experimental UV-Vis spectrum with polarization and corresponding TD-DFT (B3LYP) excitation energies (eV) from Ref. 19.

Label	exp	Polarization	TD-DFT	Assigned character
1	1.25	x,y	1.29	$d_{x^2-y^2}/d_{xy} \rightarrow d_{z^2}$
2	1.45	x,y	1.31	
3	1.61	-	0.89	Intraligand
4	1.84	z	2.01-2.07	$d_{yz}/d_{xz} \rightarrow d_{z^2}$
5	2.79	z	2.21	LMCT
-	-	-	> 3.03	MLCT[a]

[a] Not assigned experimentally

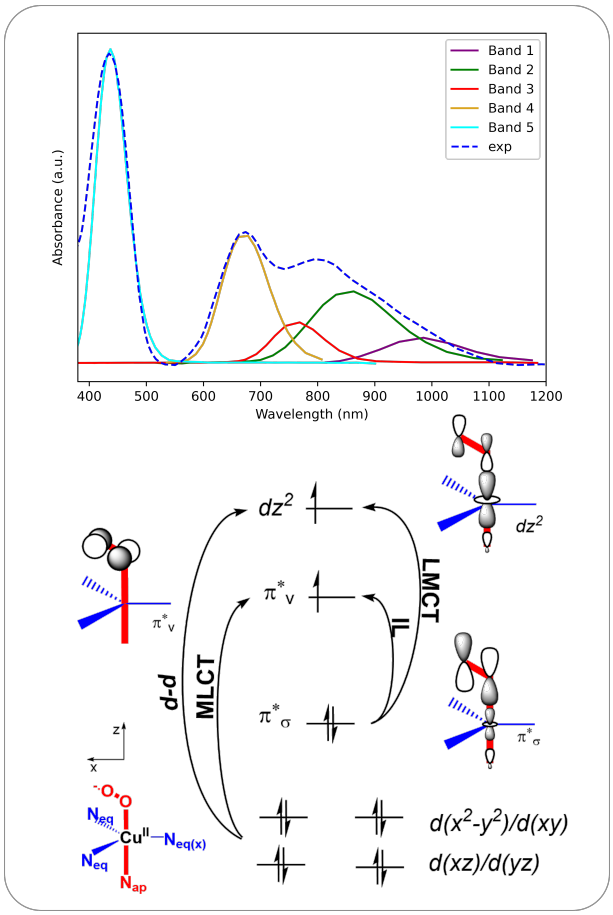

Figure 2: On top, the absorption spectrum of a $[(TMG_3tren)Cu(O_2)]^+$ complex and its deconvolution into the five identified bands. Reproduced from Ref.[19] Copyright 2010 American Chemical Society. At the bottom, a simplified molecular orbital diagram, indicating possible excitations.

The recording and assignment of the electronic absorption spectrum of copper(II) superoxido complexes in a trigonal bipyramid environment can be traced back to the seminal work by Woertink et al. on $[(TMG_3tren)Cu(O_2)]^+$.[19] It consists of five bands as shown in Figure 2, and can be understood on the basis of the molecular orbital picture of the complex, composed of the four doubly occupied copper d orbitals, the π^*_σ doubly occupied orbital, mostly localized on the dioxygen, and the two SOMOs, usually referred to as the copper d_{z^2} and the dioxygen π^*_v orbitals. The absorption spectrum was interpreted as follows: a group of $d-d$ transitions (bands 1, 2, 4 in Table 1); the LMCT band (band 5); an additional band located among the group of $d-d$ transitions (band 3). The assignment of the spectrum was achieved thanks to a combined experimental and TD-DFT study, which included Magnetic Circular Dichroism (MCD) and Resonance Raman (rR) experiments. Band 3 was introduced to account for the intensity between bands 2 and 4, but it has very low MCD intensity. The rR profile of the complex reveals an enhancement of the O-O mode $\nu(O-O)$ in band 3, but not of the Cu-O mode $\nu(C-O)$. Thus, the possibility that band 3 corresponds to an MLCT (Metal to Ligand Charge Transfer) transition was disregarded (insensitive to $\nu(C-O)$) and the band was attributed to the Intraligand (IL) transition implicating the antibonding orbitals of the dioxygen moiety.[19]

As TD-DFT displays well-known deficiencies for the description of charge-transfer excitations, double excitations and transitions implicating excited states with high multiconfigurational character, a full agreement could not be achieved between theory and experiment.[19,24] Band 3 was attributed to the IL transition, despite a large difference in absorp-

tion energies (λ_{exp} = 769 nm or 1.61 eV vs. λ_{TDDFT} = 1389 nm or 0.89 eV). Its assignment was and continues to be inconclusive.

With its nine valence electrons, the open-shell copper(II) cation has a compact, crowded, but not completely full 3*d*-shell. Even if the presence of the ligand field reduces near-degeneracy issues, this family of copper complexes is considered 'tough' for computational treatments.[13,25–29] We can expect the ground and excited states to exhibit at least some degree of multiconfigurational character that needs to be accounted for in the theoretical treatment. To the best of our knowledge, there are no wavefunction based studies on the spectroscopy of the bipyramid trigonal copper(II) superoxido complexes. With recently developed high-performance implementations of DMRG (Density Matrix Renormalization Group) in `BLOCK2`,[30] and compact selected-CI schemes, such as ICE-CI (Iterative Configuration Expansion - Configuration Interaction) in `ORCA`,[31,32] multireference calculations can be performed in a reasonable time even with the large active spaces needed for this class of complexes. There is however no well-established way of performing dynamic correlation treatments in these cases. The cost associated with the scaling of the DMRG-based perturbation theory treatment is prohibitive, and approximate schemes have been shown to lead to potential intruder states.[33,34] Selected-CI schemes, which can provide explicit wavefunction coefficients for large configuration spaces, can be extremely useful to provide a clear picture of the correlation mechanisms at play in the most challenging cases.

In this work we shall focus on end-on copper(II) superoxido complexes with a triplet ground state. The systems considered are shown in Figure 1. We provide an in-depth study of the $[(\text{tren})\text{Cu}(\text{O}_2)]^+$ complex, as a model system for the $[(\text{TMG}_3\text{tren})\text{Cu}(\text{O}_2)]^+$ and $[(\text{TMPA})\text{Cu}(\text{O}_2)]^+$ complexes. Multireference calculations on the large $[(\text{TMPA})\text{Cu}(\text{O}_2)]^+$ have also been performed. To better highlight the role of the bipyramid trigonal environment on the electronic structure of the complex, we extend the comparison to $[(\text{NH}_3)\text{Cu}(\text{O}_2)]^+$. Calculations were performed with several multireference methods. As we are constrained by their high computational cost, their combined use allows us to access complementary information and to provide a convincing picture of the electronic structures of the complexes. Perturbation theory applied to a RASSCF (Restricted Active Space Self-Consistent Field) reference wavefunction is a good compromise between accuracy and computational cost.[25] The MS-RASPT2 (Multi-State Restricted Active Space Perturbation Theory at 2nd order) approach available in `OpenMolcas` offers a robust way to describe vertical transitions between states of high multiconfigurational character.[35,36] In addition, we used an approximate Full-CI solver (DMRG) to assess the effects of hole/particle restrictions in the active space within the RASSCF approach. Finally, selected-CI calculations are exploited to gain a better understanding of the nature of the ground and excited states, and evaluate the influence of including some of the tren ligand orbitals in the active space.

We provide an interpretation of the results using quantitative metrics based on the 1-TDM (1-electron Transition Density Matrix) and wavefunction analysis to evaluate the nature of the transitions.[37,38] This allows us to propose a revised interpretation of the spectrum.

Methodology

Computational details

Geometry optimizations were performed with the `Turbomole 7.5` package,[39] at the DFT level using the PBE0-D3 functional,[40–44] with a def2-QZVPP basis set on the Cu center and a def2-TZVP basis set on remaining atoms in all cases.[45,46] The RI-J technique was used,[47,48] with the corresponding auxiliary basis functions.[49] Relevant computed geometrical parameters are reported in Table 2. In the case of $[(\text{NH}_3)\text{Cu}(\text{O}_2)]^+$, the lack of the equatorial co-

Table 2: Computed geometrical parameters of the studied complexes (distances in pm, angles in degrees), PBE0-D3 optimized structures. Labels as in Figure 2.

Complex	Cu-O	Cu-N_{ap}	O-O	Cu-$N_{eq(x)}$	Cu-O-O	O-O-Cu-N_{eq}
$[(tren)Cu(O_2)]^+$	195.7	219.0	125.0	211.6	108.9	-62.5
$[(TMPA)Cu(O_2)]^+$	193.7	218.5	125.3	206.2	112.7	-59.8
$[(TMG_3tren)Cu(O_2)]^+$	195.0	218.8	127.3	211.2	119.5	-49.6
$[(NH_3)Cu(O_2)]^+$	192.6	193.7	119.8	-	129.8	-

ordination sphere impacts the global structure of the complex: the Cu-N_{ap} distance (between the copper center and the apical nitrogen atom, see Figure 2 for labels) is sensibly shorter than in the other complexes. The coordination of the O_2 is also affected, as revealed by the short O-O distance.

Concerning the choice of the systems, the $[(tren)Cu(O_2)]^+$ complex is a good model for copper(II) superoxido complexes in a trigonal bipyramid environment: as can be seen in Table 3, it possesses a characteristic LMCT band at the TD-DFT level comparable to those of the $[(TMG_3tren)Cu(O_2)]^+$ and $[(TMPA)Cu(O_2)]^+$ complexes. The other low-lying electronic transitions are also of similar nature. Moreover, from an experimental point of view, the absorption spectrum of $[(Me_6tren)Cu(O_2]^+$ and $[(TMPA)Cu(O_2)]^+$ complexes were reported in propionitrile and they display very close features (λ_{max} at 412 and 414 nm, respectively).[17]

Table 3: Experimental[19,21] and computed LMCT band for four copper(II) superoxido (PBE0-D3, Tamm-Dancoff approximation). ΔE in eV and λ in nm.

Complex	ΔE (λ) exp.	ΔE PBE0-D3
$[(tren)Cu(O_2)]^+$	-	2.75
$[(TMPA)Cu(O_2)]^+$	2.93 (423)	2.66
$[(TMG_3tren)Cu(O_2)]^+$	2.79 (444)	2.54

Average RASSCF calculations were performed on the PBE0-D3 geometries with `OpenMolcas 22.02`,[35,36] using the Cholesky decomposition of the two-electron integrals (RICD) with a threshold of 10^{-6} hartree.[50,51] Core electrons ($1s$ shell for C, N and O atoms, and $1s2s2p$ shells for Cu) were kept frozen in all RASSCF calculations. The IPEA (Ionization Potential Electron Affinity) shift with the standard value of 0.25 hartree was applied throughout.[52] Moreover, an imaginary shift of 0.1 hartree was introduced to prevent intruder states.[53] RASPT2 and MS-RASPT2 were applied on top of the average RASSCF calculations. DMRG calculations were performed on the same structures using `BLOCK2 0.5`,[30] interfaced with `PySCF 2.1.1`.[54] In that case, the density fitting procedure with autogenerated auxiliary basis sets was used.[55] DMRG-NEVPT2 calculations were also performed (Supporting Information), but not used, because too low energies were obtained for the LMCT with the approximate compressed NEVPT2 scheme.[56,57] RASSCF-based and DMRG calculations were performed using the ANO-R3 basis set.[58] Scalar relativistic effects were included using the X2C formalism.[59] In all the cases mentioned above, the wavefunction was optimized on average for the states of interest, in order to obtain the overall spectrum up to the LMCT band. Selected CI were performed with `ORCA 5.0`,[31,32,60] using the CSF-based (Configuration State Function) version of the ICE-CI program along with the def2-SVP basis set.[45,46] For this particular case, localized orbitals were used and obtained following the New-Boys procedure. Transition density matrix analysis was performed with the `TheoDORE 3.0` toolbox for excited states and the `libWFA` library.[37,61] For completeness, TD-DFT results for all complexes are reported in the Supporting Information.

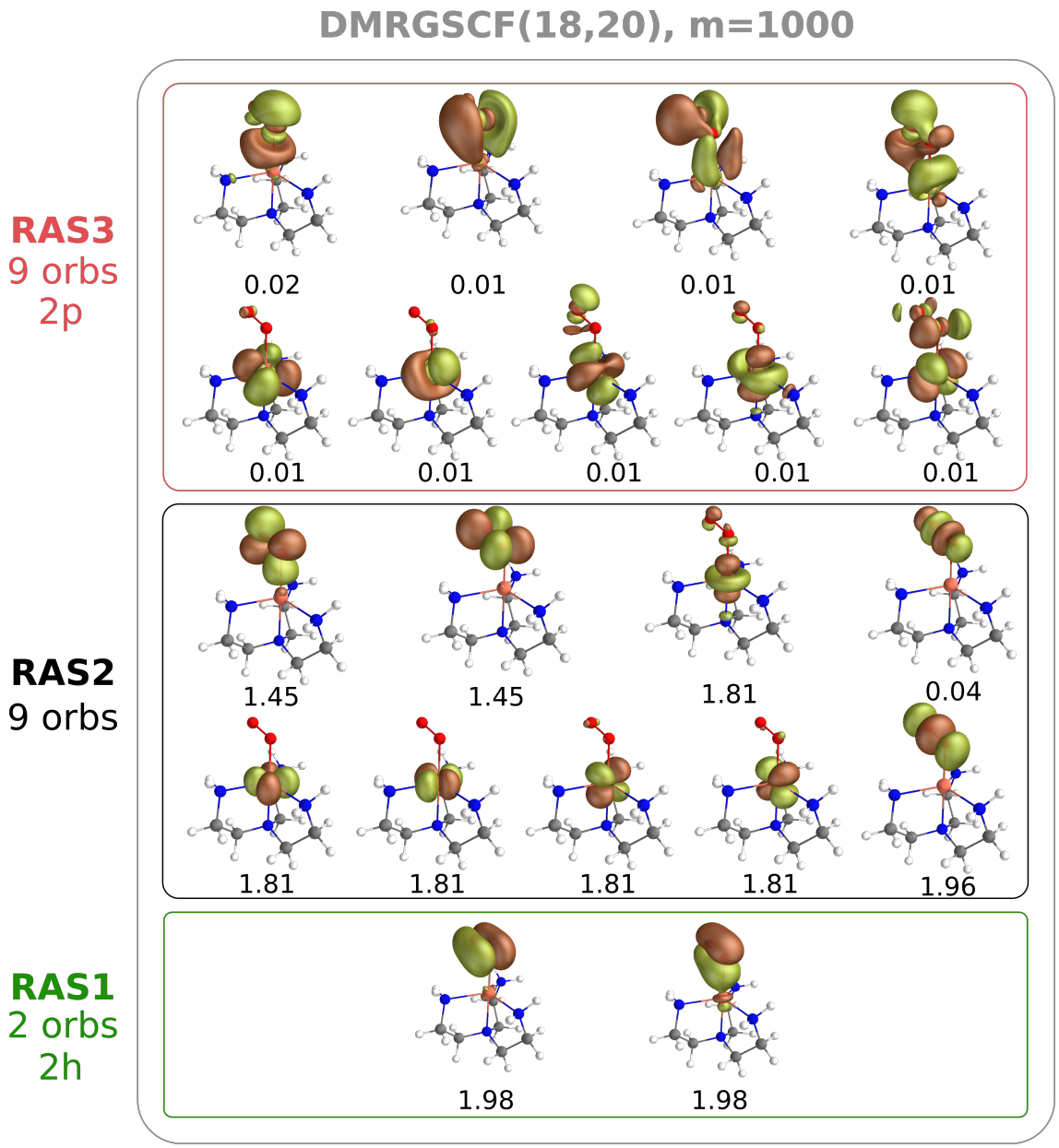

Figure 3: Active space of $[(\text{tren})\text{Cu}(\text{O}_2)]^+$, average natural orbitals of RAS(18,2,2;2,9,9).

Active space selection for RAS, DMRG and ICE-CI

In the choice of the active space, to keep the system tractable, we limited ourselves to the most significant orbitals for the problem at hand,[62,63] and resorted to using a RASSCF wavefunction. The selected active space for the $[(\text{tren})\text{Cu}(\text{O}_2)]^+$ complex is a RAS(18,2,2;2,9,9). It contains 18 electrons in three orbital subspaces (RAS1, RAS2, RAS3) and only double excitations out of RAS1 and into RAS3 are allowed, while a full CI is performed in the RAS2. The subspaces, shown in Figure 3, are built as follows: the bonding π-orbitals of the dioxygen are confined to the RAS1 subspace (2 orbitals); the RAS2 includes the remaining dioxygen orbitals built on the $2p$ shells and the $3d$ orbitals of the copper (9 orbitals). The double-d shell effects are treated in the RAS3 and a double shell for the dioxygen moiety is also partially included with four correlating orbitals, analogous to the two antibonding π^* orbitals of O_2 (9 orbitals).[25] One of them exhibits a strong copper $4s$ character. The inclusion of the $3p$ double shell of dioxygen is necessary to obtain accurate energies for the LMCT band. Thus, the active

space includes all the significant metal orbitals, together with the π- and σ-like dioxygen orbitals built on the $2p$ shells and partial double shells. We neglected the coordinating orbitals of nitrogen atoms from the tren moiety, as their inclusion in the active space renders the following perturbation treatment too costly. Doubly occupied inactive orbitals were kept frozen during the perturbation treatment. Their inclusion leads to intruder state problems for the ground state root and the LMCT in particular (Table S9 in the Supporting Information).

The need for a double shell is well known for 1st row transition metals and its importance for computing accurate energy differences has been highlighted earlier.[62] In a previous work, it has been shown that a partial treatment of the double shell effects using the RASSCF approximation was sufficiently accurate most of the time.[64] In order to evaluate these effects and rule out other potential biases arising from the hole/particle restrictions, we performed a DMRG calculation on an active space of same nature as in Figure 3. DMRGSCF with a CAS(18,20) on 11 roots was carried out with increasing bond dimension m from 100 to 1000. A perturbative noise correction was applied in the first sweeps to improve the convergence. An additional DMRGCI calculation with $m = 2000$ was performed on the seemingly well converged orbitals at $m = 1000$. Extrapolation was performed for the ground state root using a reverse sweep schedule. It shows that for $m = 2000$, the ground state energy differs by only 0.04 mhartree from the DMRG energy at infinite bond dimension. We report an additional DMRGSCF calculation with a CAS(20,23) for $[(\text{tren})\text{Cu}(\text{O}_2)]^+$, where the apical nitrogen σ-donor orbital was included in the active space with the corresponding virtual correlating orbital as well as an in-phase combination of $3p$ orbitals on the dioxygen moiety.

Setting aside the computational cost considerations, the hypothesis behind leaving tren orbitals out of the active space is that a perturbative treatment on a large enough reference space should be able to recover the correlation effects necessary to yield reasonable energy differences. To address this question, and rule out any bias introduced by the state-averaging procedure on a limited number of states, a selected CI approach (ICE-CI) was used on a CAS(34,35) wavefunction. These enlarged active space, chosen after a molecular orbital localization, includes in addition semicore $3s3p$ and virtual $4s$ of Cu, nitrogen pairs of the tren ligand together with their virtual counterpart, and the full $3p$ shell of dioxygen. In that case, we used threshold values of $T_{gen} = 10^{-4}$ and $T_{var} = 10^{-9}$ leading a total of 9.1 million CSFs. The detailed procedure used to set up the calculations is reported in the Supporting Information, as well as all mentioned active spaces.

Calculations for the $[(\text{TMPA})\text{Cu}(\text{O}_2)]^+$ complex were performed using a similar RAS(18,2,2;2,9,9) active space as for the $[(\text{tren})\text{Cu}(\text{O}_2)]^+$ complex. For the $[(\text{NH}_3)\text{Cu}(\text{O}_2)]^+$ complex, a RAS(20,2,2;3,10,9) active space was chosen: it includes as well the apical nitrogen orbital in the RAS1 and the copper $4s$ orbital in the RAS2. In the DMRG calculation, we used the same CAS(20,23) as previously described for $[(\text{tren})\text{Cu}(\text{O}_2)]^+$.

Results and Discussion

Results of wavefunction methods

We present results for three $[\text{CuO}_2]^+$ complexes, $[(\text{tren})\text{Cu}(\text{O}_2)]^+$, $[(\text{TMPA})\text{Cu}(\text{O}_2)]^+$ and $[(\text{NH}_3)\text{Cu}(\text{O}_2)]^+$, in terms of energy differences ΔE with respect to the triplet ground states. In order to compare results, we follow, for all methods, the ordering of the states found at the MS-RASPT2 level of theory, Tables 4-5. For each root, we indicate the main electronic configuration and its weight in the RASSCF wavefunction. For the ICE-CI wavefunction, the assignment is based on the CSF with the highest weight in the localized orbital basis. The ground state spin densities of these triplet complexes are shown in Figure 4. The spin densities of the excited states are available in the Supporting Information, as well as the CSFs' weights (Table S4) and their schematic

representation.

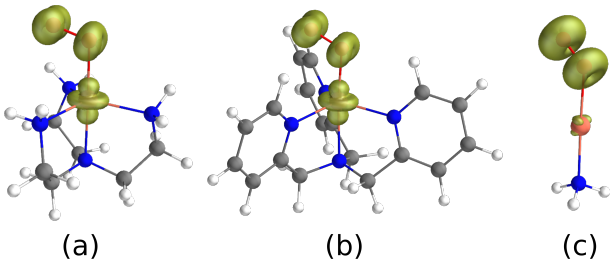

Figure 4: Ground state spin densities of complexes (a) $[(\text{tren})\text{Cu}(\text{O}_2)]^+$, (b) $[(\text{TMPA})\text{Cu}(\text{O}_2)]^+$, and (c) $[(\text{NH}_3)\text{Cu}(\text{O}_2)]^+$.

$[(\text{tren})\text{Cu}(\text{O}_2)]^+$

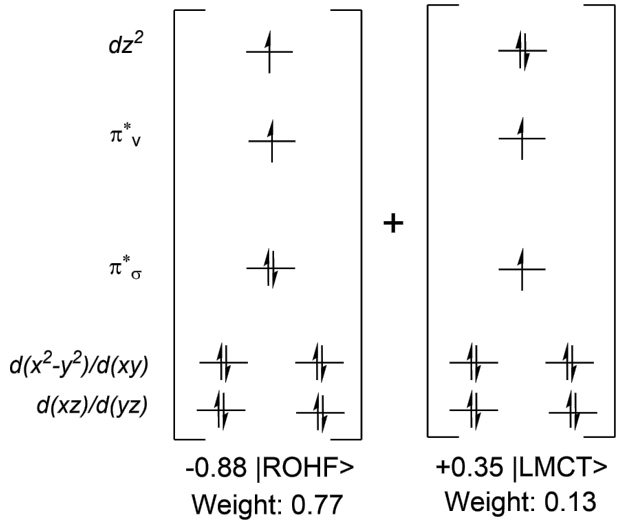

Figure 5: Schematic representation of the major CSFs of the $[(\text{tren})\text{Cu}(\text{O}_2)]^+$ ground state T0.

Concerning the $[(\text{tren})\text{Cu}(\text{O}_2)]^+$ complex, Table 4, the ground state is found to be predominantly the combination of the $|ROHF\rangle$ and $|LMCT\rangle$ CSFs, with a weight of 0.77 and 0.13, respectively, as schematically depicted in Figure 5. The first transition corresponds to the IL. A group of 8 states follows, which are within a 0.5-0.6 eV range depending on the method. Interestingly, it consists of $d-d$ excitations, but also of doubly excited states with respect to the main CSF of the ground state (the $|ROHF\rangle$). These correspond to the removal of electrons from doubly occupied d orbitals and the π^*_σ to populate the SOMOs (π^*_v and d_{z^2}). They can be seen either as combined MLCT and LMCT transitions, or as simultaneous IL and $d-d$. The LMCT state is the eleventh root, T10. Satisfyingly, all wavefunction methods agree on the global trends, although some inversions are observed for near-degenerate states. By comparing RASSCF and DMRG in Table 4, we observe that the results are in good agreement: differences in ΔE for the IL, $d-d$ transitions and double excitations are small, within a 0.09-0.12 eV range. Effects on the LMCT are somewhat larger, as in this case the DMRG excitation energy (3.626 eV) is found to be lower by 0.63 eV than the corresponding RASSCF value (4.258 eV). This LMCT state involves a change of the metal oxidation state from Cu^{II} to Cu^{I} and the DMRG treatment allows for more flexibility in the wavefunction to accommodate for this change than a RASSCF approach. DMRG with a larger CAS(20,23) leads to comparable results as can be seen in Table S11 in the Supporting Information.

Confident that our RASSCF behaves correctly, we treat the remaining correlation effects using both the state-specific (RASPT2) and multi-state (MS-RASPT2) approaches. Introducing dynamical correlation with the perturbative treatment has the following effect: similarly to the trend observed by moving from RASSCF to DMRG, excitation energies for the IL and $d-d$ transitions slightly increase with respect to the values obtained at the RASSCF level, while the LMCT band is found at a significantly lower energy. The effects of the multi-state treatment are non-negligible as all states show a relatively high degree of mixing. It has an impact on the ordering of the $d-d$ and doubly excited transitions, which involve pairs of nearly degenerate d orbitals, with contributions ranging from 0.06 to 0.09 eV. The most affected state is the double excitation T4, which is heavily mixed. MS-RASPT2 shifts this state between two blocks of nearly degenerate $d-d$ transitions, while RASPT2 would locate it higher in energy, after the $d-d$ transitions. The LMCT state is also affected and the MS-RASPT2 treatment further increases the energy difference with the ground state by 0.24 eV with

Table 4: Vertical excitation energies (ΔE in eV) of $[(\text{tren})\text{Cu}(\text{O}_2)]^+$ at different levels of theory, the order follows that of MS-RASPT2 calculations. The weight corresponds to the square of the coefficient of the highest contributing CSF in the RASSCF wavefunction.

State	Main CSF (weight)	MS-RASPT2 RAS(18,2,2;2,9,9)	RASPT2 RAS(18,2,2;2,9,9)	RASSCF RAS(18,2,2;2,9,9)	DMRG CAS(18,20)	ICE-CI CAS(34,35)
T0	$\|ROHF\rangle$ (0.77)	0.000	0.000	0.000	0.000	0.000
T1	$\|IL\rangle$ (0.92)	1.006	0.912	0.741	0.843	0.837
T2	$d_{x^2-y^2} \rightarrow d_{z^2}$ (0.50)	1.371	1.289	1.141	1.237	1.500
T3	$d_{xy} \rightarrow d_{z^2}$ (0.56)	1.433	1.339	1.185	1.290	1.583
T4	$d_{yz}, \pi^*_\sigma \rightarrow d_{z^2}, \pi^*_v$ (0.47)	1.591	1.530	1.394	1.483	1.663
T5	$d_{yz} \rightarrow d_{z^2}$ (0.57)	1.608	1.514	1.352	1.458	1.801
T6	$d_{xz} \rightarrow d_{z^2}$ (0.54)	1.637	1.543	1.379	1.487	1.832
T7	$d_{x^2-y^2}, \pi^*_\sigma \rightarrow d_{z^2}, \pi^*_v$ (0.60)	1.771	1.678	1.492	1.611	1.782
T8	$d_{xy}, \pi^*_\sigma \rightarrow d_{z^2}, \pi^*_v$ (0.59)	1.905	1.820	1.638	1.752	1.944
T9	$d_{xz}, \pi^*_\sigma \rightarrow d_{z^2}, \pi^*_v$(0.61)	1.990	1.896	1.704	1.823	2.055
T10	$\|LMCT\rangle$ (0.68)	2.845	2.604	4.258	3.626	3.139

respect to the state-specific case (Table 4). Another active space including a $4d_{yz}$ orbital in the RAS2 was also tested initially and leads to comparable results reported in the Supporting Information.

Finally, although a smaller basis set was employed, ICE-CI results are in very good agreement with those at the MS-RASPT2 level. We conclude that our MS-RASPT2 approach, using a smaller and restricted active space, is suitable to retrieve the correct state ordering and account for contributions from the tren moiety and semi-core electrons of the metal, explicitly included in the ICE-CI treatment.

$[(\text{TMPA})\text{Cu}(\text{O}_2)]^+$

Values computed for the $[(\text{TMPA})\text{Cu}(\text{O}_2)]^+$ complex at the MS-RASPT2 level, are reported in Table 5. The results are comparable to those obtained for the $[(\text{tren})\text{Cu}(\text{O}_2)]^+$ complex. Except for a few minor inversions for near-degenerate states, the ordering is the same. The IL band is found at an even lower energy than in the $[(\text{tren})\text{Cu}(\text{O}_2)]^+$ complex. The $d-d$ transitions are underestimated at the MS-RASPT2 level with respect to the recorded experimental values of 1.64 and 2.12 eV.[21] However, in this case, the computed LMCT band is found at 3.08 eV, which is only a slight overestimation with respect to the experimental value of 2.93 eV.[21]

$[(\text{NH}_3)\text{Cu}(\text{O}_2)]^+$

Moving forward, we now turn our attention to the MS-RASPT2 results for the ten lowest excited states of the $[(\text{NH}_3)\text{Cu}(\text{O}_2)]^+$ complex, displayed in Table 5.

As can be seen in Figure 4, the electronic structure of the ground state differs from that of the bipyramid trigonal complexes. For T0, the spin density is exclusively located on the dioxygen. The first excited state consists here of a MLCT transition from the bioccupied d_{z^2} orbital to the π^*_z SOMO orbital as represented in the molecular orbital diagram of Figure 6. The remaining transitions are also MLCT from a d orbital to

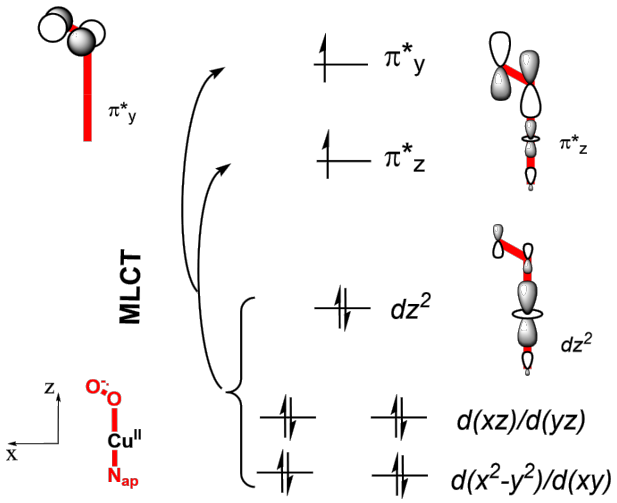

Figure 6: Molecular orbital diagram of $[(\text{NH}_3)\text{Cu}(\text{O}_2)]^+$ showing possible excitations.

Table 5: MS-RASPT2 vertical excitation energies (ΔE in eV) of $[(TMPA)Cu(O_2)]^+$, RAS(18,2,2;2,9,9), and $[(NH_3)Cu(O_2)]^+$, RAS(20,2,2;3,10,9). The weight corresponds to the square of the coefficient of the highest contributing CSF in the RASSCF wavefunction.

	$[(TMPA)Cu(O_2)]^+$		$[(NH_3)Cu(O_2)]^+$	
State	Main CSF (weight)	ΔE	Main CSF (weight)	ΔE
T0	$\|ROHF\rangle$ (0.77)	0.000	ROHF (0.70)	0.000
T1	$\|IL\rangle$ (0.92)	0.896	$d_{z^2} \rightarrow \pi_z^*$ (0.88)	2.829
T2	$d_{xy} \rightarrow d_{z^2}$ (0.67)	1.262	$d_{yz} \rightarrow \pi_z^*$ (0.88)	3.322
T3	$d_{x^2-y^2} \rightarrow d_{z^2}$ (0.62)	1.276	$d_{xz} \rightarrow \pi_z^*$ (0.83)	3.411
T4	$d_{xy}, \pi_\sigma^* \rightarrow d_{z^2}, \pi_v^*$ (0.43)	1.389	$d_{z^2} \rightarrow \pi_y^*$ (0.88)	3.583
T5	$d_{yz} \rightarrow d_{z^2}$ (0.39)	1.523	$d_{xy} \rightarrow \pi_z^*$ (0.86)	3.603
T6	$d_{xz} \rightarrow d_{z^2}$ (0.57)	1.531	$d_{x^2-y^2} \rightarrow \pi_z^*$ (0.83)	3.604
T7	$d_{x^2-y^2}, \pi_\sigma^* \rightarrow d_{z^2}, \pi_v^*$ (0.35)	1.578	$d_{xz} \rightarrow \pi_y^*$ (0.81)	4.206
T8	$d_{yz}, \pi_\sigma^* \rightarrow d_{z^2}, \pi_v^*$ (0.46)	1.764	$d_{yz} \rightarrow \pi_y^*$ (0.74)	4.235
T9	$d_{xz}, \pi_\sigma^* \rightarrow d_{z^2}, \pi_v^*$(0.75)	1.847	$d_{xy} \rightarrow \pi_y^*$ (0.65)	4.446
T10	$\|LMCT\rangle$ (0.69)	3.083	$d_{x^2-y^2} \rightarrow \pi_y^*$ (0.81)	4.447

the π_z^* SOMO (3.3 $\rightarrow$ 3.6 eV, T2, T3 and T4 at the MS-RASPT2 level) or the π_y^* (3.6 $\rightarrow$ 4.4 eV, T4, T7- T10). The transition from the higher lying d_{z^2} orbital to the π_y^* orbital T4 is slightly lower in energy than the other $d \rightarrow \pi_y^*$ transitions.

Discussion

Analysis of the states

We shall now discuss the nature of the relevant states for $[(NH_3)Cu(O_2)]^+$, $[(tren)Cu(O_2)]^+$ and $[(TMPA)Cu(O_2)]^+$. Some insights are easily accessible by comparing the partial charges computed on the metal center and oxygen atoms, available in Table 6. The charge on the copper significantly increases from the ground state of $[(NH_3)Cu(O_2)]^+$ to $[(tren)Cu(O_2)]^+$, in line with the schematic representation of the molecular orbitals proposed in Figure 7. Although this picture provides a very simplified view of the electronic structure of these two complexes, it helps to understand their key differences.

In the $[(NH_3)Cu(O_2)]^+$ complex, due to the presence of only one nitrogen based ligand, the d_{z^2}-like orbital in the $[(NH_3)Cu]^+$ fragment is rather low in energy. Two molecular orbitals are obtained through interaction with the dioxygen. The lowest one, which is doubly occupied and formally the Cu-O bonding orbital, is mostly localized on the copper. In the case of the $[(tren)Cu(O_2)]^+$ complex, a more complete coordination sphere around the metal pushes copper d-like orbitals up in energy. Thus, the highest doubly occupied molecular orbital, again formally the Cu-O bonding orbital built by combining π^* and d_{z^2} orbitals, is mostly localized on the dioxygen moiety, while the antibonding d_{z^2}-like orbital remains monooccupied.

Interestingly, the charges (LoProp)[65] computed for the ground state of the $[(tren)Cu(O_2)]^+$ complex are similar to those of the $[(NH_3)Cu(O_2)]^+$ first and second excited states (T1 and T2). This illustrates that, in the case of the $[(NH_3)Cu(O_2)]^+$ complex, the electronic density is displaced away from the copper center in the excited state. On the other hand, the charges computed for the LMCT transition in $[(tren)Cu(O_2)]^+$ are similar to those of the ground state of $[(NH_3)Cu(O_2)]^+$. We note that the partial charges obtained for the reported $d-d$ transition (T3) and the double excitation (T4 and T7) in $[(tren)Cu(O_2)]^+$ are roughly the same as in the ground state, suggesting that they do not imply a significant charge transfer. This also holds true for the other transitions of the same kind, see Supporting Information for more details.

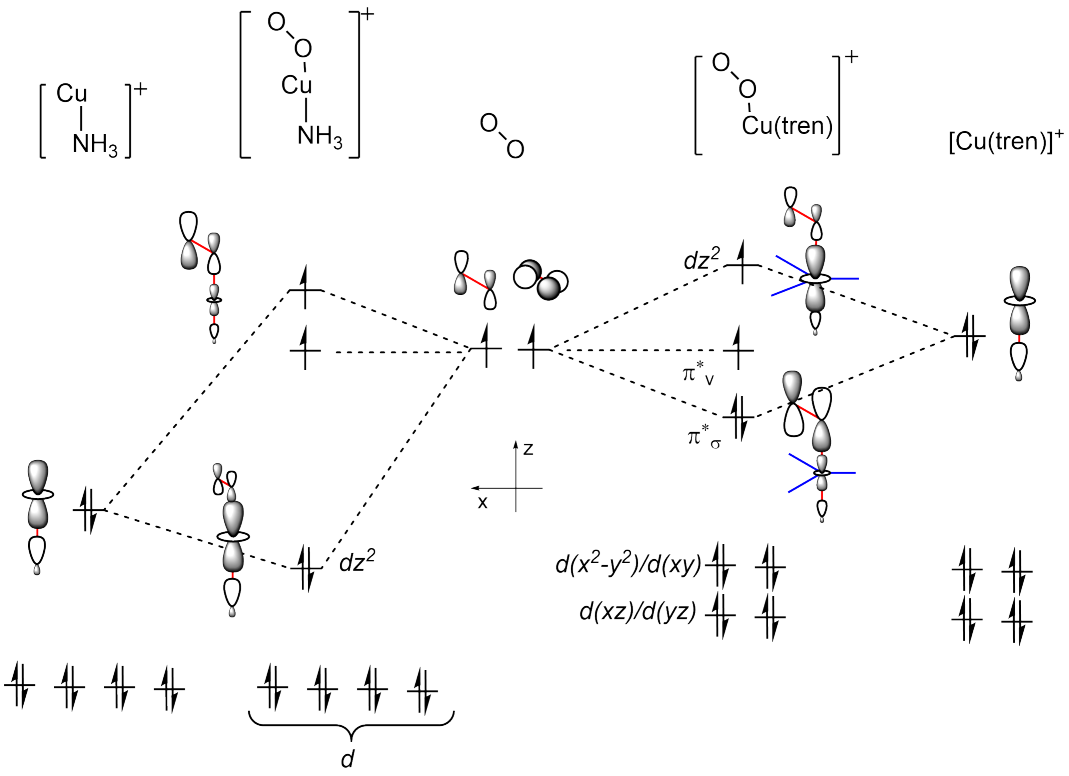

Figure 7: Schematic molecular orbital diagram for $[(NH_3)Cu(O_2)]^+$ and $[(tren)Cu(O_2)]^+$, constructed from the fragments O_2 (in the center) and $[(NH_3)Cu]^+$ (on the left) or $[(tren)Cu(O_2)]^+$ (on the right). Energies are arbitrary.

Table 6: Charges per center from the RASSCF wavefunctions (LoProp),[65] O_a is the oxygen atom bound to copper.

	$[(NH_3)Cu(O_2)]^+$			$[(tren)Cu(O_2)]^+$				
	T0	T1	T2	T0	T3	T4	T7	T10 (LMCT)
Cu	0.69	1.21	1.23	1.22	1.35	1.34	1.36	0.58
O_a	-0.05	-0.33	-0.33	-0.38	-0.48	-0.49	-0.50	-0.05
O_b	0.12	-0.11	-0.11	-0.28	-0.30	-0.27	-0.29	0.04

For the tren case, we refine the analysis of the nature of each transition by using the tools available in the `TheoDORE` suite. From the 1-TDM computed with RASSI on the perturbed MS-RASPT2 wavefunction, we obtain the hole and electron densities using singular value decomposition. The (Hole/Electron) density plots give a pictorial representation of the transitions. Moreover, a fragment analysis on the transformed 1-TDM (in the AO basis) allows us to quantify the amount of charge transfer for the different excitations, Figure 8.[37,38] In our case, we define three interacting fragments: the metal, dioxygen and tren ligand. In Figure 8, the value of the ordinate will vary depending on the one-electron character of the transition, for a pure single excitation it will be exactly one, for a pure double excitation it will be zero. The 1-TDM is obtained by integrating out all but a single electron and it catches the nature of transitions due to mono-excitations. It does not contain information about the two-electron or higher contributions to the wavefunction. When these contributions are relevant, the (Hole/Electron) density plots and the fragment analysis, both based on the 1-TDM, may deliver an incomplete picture of the transitions.

According to Figure 8, the first transition $[T0 \rightarrow T1]$ is confirmed to be an IL (both electron/hole populations are on the dioxygen, in green). We identify four clear $d-d$ transi-

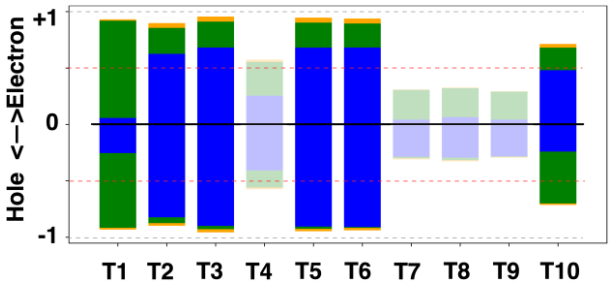

Figure 8: Fragment decomposition analysis of the 1-TDMs (RASSI on the MS-RASPT2 wavefunction, $[(\text{tren})\text{Cu}(\text{O}_2)]^+$ complex) in terms of electron/hole populations on Cu (blue), O_2 (green), and tren moieties (yellow). The shadowed histograms, with low ordinate values, concern transitions possessing double excitation contributions.

tions, $[T0 \rightarrow T2]$, $[T0 \rightarrow T3]$, $[T0 \rightarrow T5]$ and $[T0 \rightarrow T6]$ (both electron/hole populations are on the copper, in blue). The last transition $[T0 \rightarrow T10]$ is an LMCT. The assignments are supported by the (Hole/Electron) density plots for T1, T3 and T10 in Figure 9.

By inspecting Figure 8, it can be seen that the ordinate values are rather small for $[T0 \rightarrow T4]$ (approximately ± 0.5), $[T0 \rightarrow T7]$, $[T0 \rightarrow T8]$ and $[T0 \rightarrow T9]$ (approximately ± 0.25). This fact is attributed to their significant doubly excited character and suggests that both the hole-electron density plots and the fragment analysis may convey partial, limited information. We have therefore shadowed the histograms concerning these transitions in Figure 8 and the writings in the corresponding (Hole/Electron) density plots, Figure 10, to indicate that their interpretation can be misleading. The detachment and attachment densities obtained from the 1-DDM (1-electron Difference Density Matrix) provide a better picture of the overall orbital contributions for the doubly excited transitions and they are displayed for $[T0 \rightarrow T4]$ and $[T0 \rightarrow T7]$ in Figure 10.

The detachment densities suggest that electron depletion occurs simultaneously from a d orbital on the copper and the π^*_σ of the dioxygen. The attachment densities suggest an increase in electron density on both the d_{z^2} and the π^*_v. As a consequence of a compensation effect, the net global charge transfer is negligible, thus the plots indicate again that these transitions do not imply a significant charge transfer.

To evaluate such a charge transfer for each transition, we use ICE-CI calculations on a localized CASSCF wavefunction, Figure 11. The localization procedure allows us to identify three main blocks of orbitals: the copper d shell, the dioxygen p shell, and the nitrogen orbitals of the tren ligand. The remaining orbitals added in this active space were also localized separately for occupied and virtual, see Figures S15-S16 in the Supporting Information. For each state, the CSF with the highest weight is detected and referred to as "main". All the CSFs having the same number of electron per block as the main CSF are called local. Other CSFs revealing possible charge transfer contributions are classified separately. All of the contributions above a 4% threshold are plotted in Figure 11 for five states. The other states ($d-d$ and doubles) show a similar behavior. The complete data are available in the Supporting Information (Section 3.3.1).

To illustrate the meaning of these plots, we shall start by describing the ground state T0. Considering the main and local contributions as a whole, it is dominated by configurations that correspond to the ionic $\text{Cu}^{2+}\text{O}_2^{-}$ Lewis structure. Interestingly, charge transfer contributions from the dioxygen to the copper display important weights ($O_2^{2p} \rightarrow Cu^{3d}$, 19.2%), indicating a significant mixing with the LMCT state and strong covalency of the dioxygen ligand. The latter corresponds to the Cu^{+}O_2 Lewis structure where an electron is removed from the π^*_σ orbital and placed in the dz^2 orbital of the metal. This is consistent with the weights obtained with RASSCF where the $|ROHF\rangle$ configuration, corresponding to the $\text{Cu}^{2+}\text{O}_2^{-}$ structure, is predominant (Weight = 0.77), but the $|LMCT\rangle$ configuration, corresponding to the Cu^{+}O_2 structure, has a non-negligible weight of 0.13, Figure 5. The overall picture is in agreement with previous analysis of the role of LMCT on the multiconfigurational wavefunction of transition metal complexes.[26,66,67] In the case of planar copper complexes, as stated by Giner et al., it is the mixing

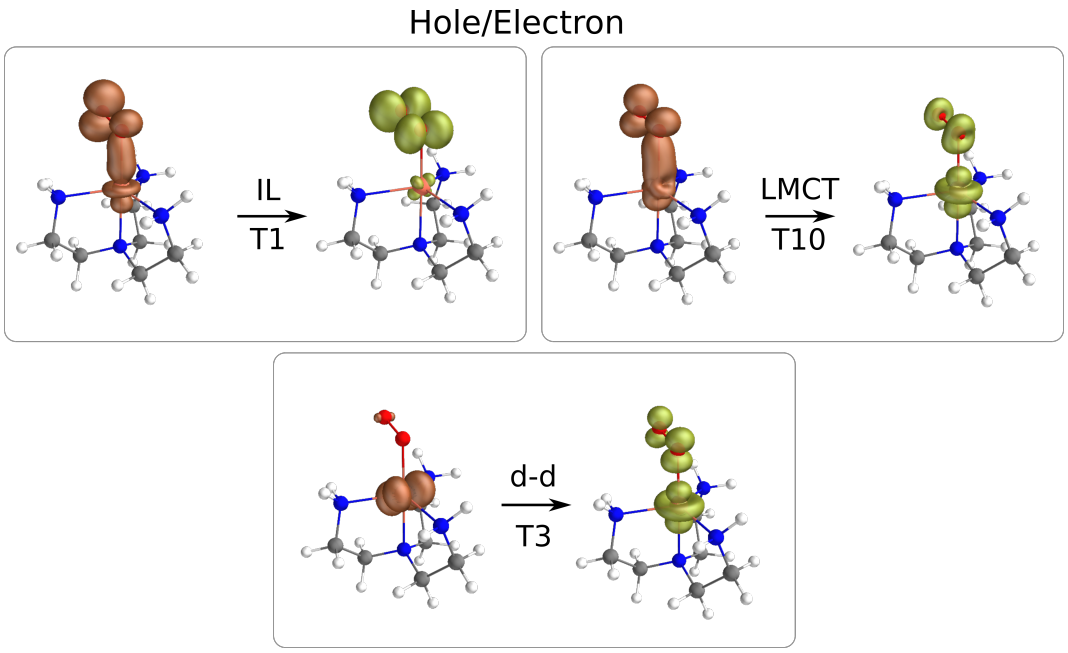

Figure 9: Hole(red)/Electron(green) densities (isovalue= 0.003) of IL, $d-d$ and LMCT (computed with RASSI on the perturbed MS-RASPT2 wavefunction).

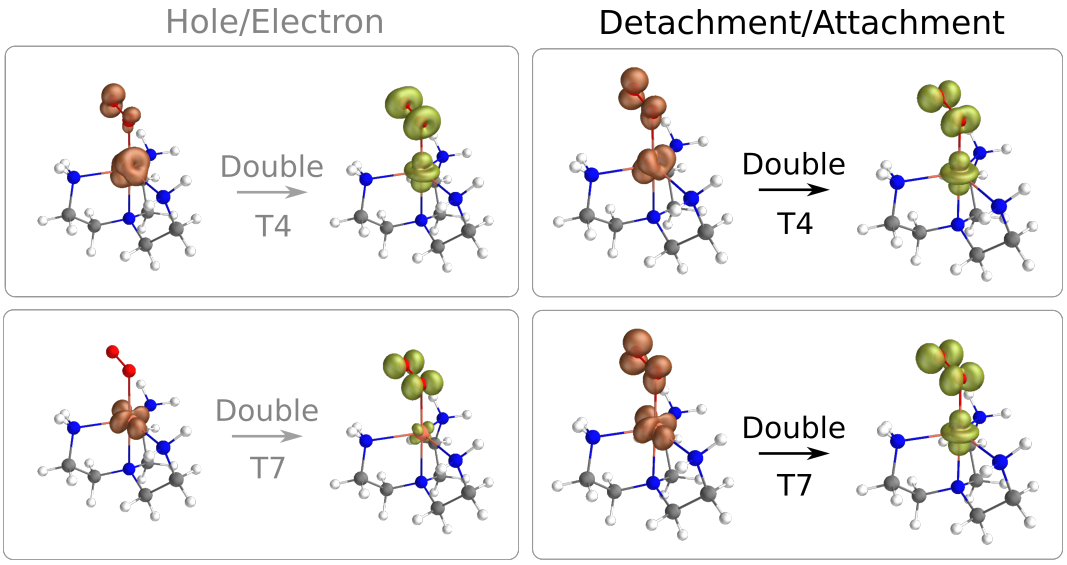

Figure 10: Hole(red)/Electron(green) densities (isovalue= 0.003) and Detachment(red)/Attachment(green) densities (isovalue= 0.02) of two transitions with significant doubly excited character (computed with RASSI on the perturbed MS-RASPT2(18,2,2;2,9,9) wavefunction).

of the Cu^{II} and Cu^{I} that yields the correct degree of ionicity of the Cu-O bond. The mixing is possible through single excitations on top of the $|LMCT\rangle$ configuration, which are important to relax the orbitals of the $|ROHF\rangle$ determinant, as the ROHF orbitals describing Cu^{2+} are not fully suitable to describe Cu^{+}. This is associated with a particular case of the "breathing orbital" effect that has been extensively described by Hiberty and coworkers.[68,69]

Let us now consider the LMCT T10 state, which is predominantly described by the $Cu^{+}O_2$ Lewis structure. For this case, the pie-chart in Figure 11 reveals significant contributions from the $3d$ shell of the metal to the $2p$ shell of the dioxygen (30.5% in red). These account for a

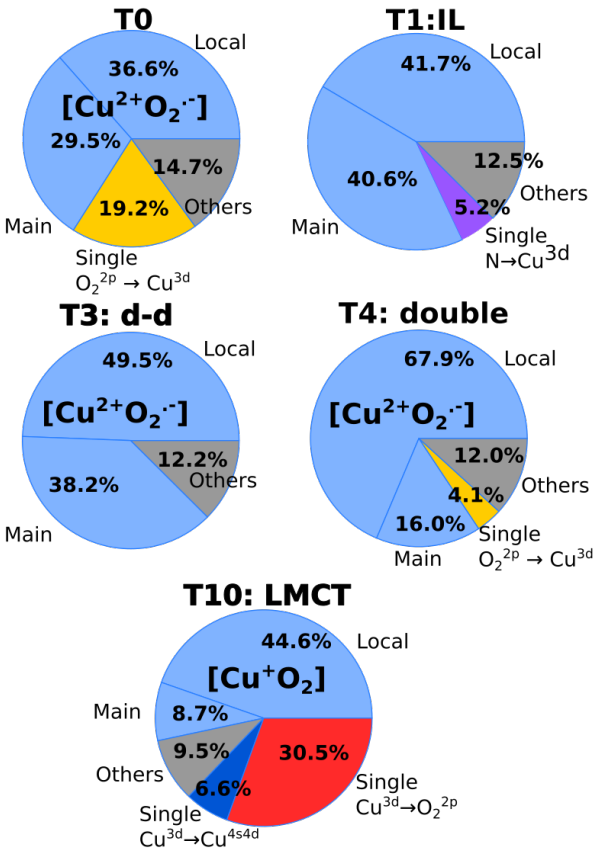

Figure 11: CSF weights of the main contributions (above 4%) to five selected roots from localized CASSCF, ICE-CI(34,35) calculation.

back-donation effect from the metal to the ligand.

The influence of charge-transfer excitations from the tren moiety are rather small in all cases. The T1 state results from the $\pi^*_\sigma \rightarrow \pi^*_v$ (IL) excitation and involves removing electron density from the Cu-O bonding orbital π^*_σ. For this case, we mention the (rather small) contribution from the tren moiety to the 3d copper orbitals (5.2%, blue region in Figure 11), which compensates the electron depletion on the metal. All remaining $d-d$ and doubly excited states show a similar profile, with no significant contribution from charge transfer configurations. In line with the fragment decomposition analysis, the state T4 shows a small charge transfer contribution from the dioxygen $2p$ shell to the metal $3d$ shell (4.1%, Figure 11).

A more in-depth analysis could be achieved by looking at the configurations' weights in the correlated wavefunctions. As reminded by Gill and coworkers,[70] the analysis of multiconfigurational wavefunctions for excited states should be subjected to caution. Given the importance of doubly excited states in our case, we disentangle the effects arising from electron correlation and orbital relaxation by performing an additional ICE-CI(34,47) calculation using the ROHF orbitals. The results are reported in the Supporting Information (Section 3.3.2) and they show that doubly excited configurations largely dominate the wavefunction of the doubly excited states.

Finally, the complex nature of the spectrum of $[(\text{tren})\text{Cu}(\text{O}_2)]^+$ is attributed to an important degree of covalency of the copper-oxygen bond. There exists a subtle interplay between close-lying π^* orbitals of the dioxygen and the $3d$ orbitals of the metal, leading to a non-negligible mixing between Cu^{II} and Cu^{I}. This gives rise to an intertwined collection of states. As the profile of $[(\text{tren})\text{Cu}(\text{O}_2)]^+$ is similar to the one of $[(\text{TMPA})\text{Cu}(\text{O}_2)]^+$ and $[(\text{TMG}_3\text{tren})\text{Cu}(\text{O}_2)]^+$, the present analysis transfers to these larger systems as well.

Interpretation of the spectrum

Having at hands all the wavefunction results, we can now test the correspondence of our model against experiment. For the $[(\text{tren})\text{Cu}(\text{O}_2)]^+$ complex, oscillator strengths were computed using the RASSI approach following the MS-RASPT2 treatment. They are displayed in Table 7. The oscillator strengths computed for the $[(\text{TMPA})\text{Cu}(\text{O}_2)]^+$ complex display similar trends as for the model $[(\text{tren})\text{Cu}(\text{O}_2)]^+$ complex, see Table S2 in the Supporting Information.

Experimental bands 1, 2, and 4 (Figure 2) were already clearly assigned to $d-d$ transitions and polarizations were given by Woertink et al.,[19] Table 1. Our wavefunction calculations recover the states that are responsible for such transitions (T2 and T3 from $d_{x^2-y^2}$ and d_{xy} to d_{z^2}; T5 and T6 from d_{yz} and d_{xz} to d_{z^2}, Table 4). The energy and nature of state T10 is

consistent with the experimental LMCT band 5 and the transition to T10 is computed to be the most intense by far from our calculations, as expected.

The assignment of band 3 to the IL transition was proposed by Woertink et al.,[19] in particular on the basis of rR experiments. However, this assignment is not trivial and can be questioned. Based on the energies that we have obtained, we are confident to say that the IL transition corresponds to state T1, which is by far the lowest excited state. This finding agrees with the TD-DFT results.[19] The computed oscillator strength of the intraligand transition is among the smallest obtained (Table 7) and this transition is expected to be dark. Thus, band 3 is too intense and too high in energy to match with the intraligand transition to T1, implicating a monoexcitation from the π^*_σ to the π^*_v orbitals of the dioxygen ligand.

Our calculations show as well that several states exist in a small 0.6 eV energy range, spanning from ΔE=1.371 eV (T2) to ΔE=1.990 eV (T9), Table 7. Besides those related to the $d-d$ transitions, the remaining four states are double excitations with respect to the $|ROHF\rangle$ CSF. According to the wavefunction results, the doubly excited states (T4, T7-T9) have a multiconfigurational nature. In T4, for example, the weights of the highest contributing CSFs are of 0.47 ($d_{yz}, \pi^*_\sigma \rightarrow d_{z^2}, \pi^*_v$) and 0.31 ($d_{xy}, \pi^*_\sigma \rightarrow d_{z^2}, \pi^*_v$) in the RASSCF wavefunction. This multiconfigurational character differs from that of T1 (the IL state), which is governed by a leading CSF, with a weight of 0.92 (see Table S4 in the Supporting Information). Importantly, these states do contain significant contributions from the π^*_σ to the π^*_v orbitals of the dioxygen, which were pointed out as essential for the state responsible of band 3.[19] The doubly excited states can be described either as a combination of $d-d$ and IL or LMCT and MLCT but not as pure MLCT or pure IL and the interpretation of the rR profiles is not straightforward. We report in the Supporting Information a preliminary study on some excited states (T1, T4 et T10) for slightly distorted structures. It suggests that state T4 is insensitive to $\nu(C-O)$ and behaves as T1 (IL) regarding $\nu(O-O)$. As such, T4 is compatible with the rR profiles. Finally, doubly excited states are expected to be dark,[71] but the multiconfigurational nature of the ground state provides a possible explanation for the non-zero intensity. Indeed, the oscillator strengths associated to these states are comparable to those of the $d-d$ transitions, Table 7. We conclude that a double excited state, such as T4, can be responsible of band 3.

Table 7: Excitation energies (ΔE in eV) and oscillator strengths, in the length (f_{len}) and velocity (f_{vel}) representations, of the $[(\text{tren})\text{Cu}(\text{O}_2)]^+$ excited states, as computed at the MS-RASPT2 level for the RAS(18,2,2;2,9,9) active space, we follow here the MS-RASPT2 ordering.

		RAS(18,2,2;2,9,9)		
		ΔE	f_{len}	f_{vel}
T1	IL	1.006	$< 10^{-5}$	$1.5 \cdot 10^{-4}$
T2	$d-d$	1.371	$3.0 \cdot 10^{-3}$	$5.2 \cdot 10^{-3}$
T3	$d-d$	1.433	$2.3 \cdot 10^{-5}$	$1.3 \cdot 10^{-4}$
T4	double	1.591	$9.2 \cdot 10^{-3}$	$8.9 \cdot 10^{-3}$
T5	$d-d$	1.608	$5.0 \cdot 10^{-5}$	$2.9 \cdot 10^{-4}$
T6	$d-d$	1.637	$7.4 \cdot 10^{-5}$	$3.8 \cdot 10^{-4}$
T7	double	1.771	$1.3 \cdot 10^{-5}$	$1.1 \cdot 10^{-4}$
T8	double	1.905	$2.6 \cdot 10^{-3}$	$1.6 \cdot 10^{-3}$
T9	double	1.990	$< 10^{-5}$	$< 10^{-5}$
T10	LMCT	2.845	$1.5 \cdot 10^{-1}$	$1.3 \cdot 10^{-1}$

Conclusion

Ground and excited states of triplet bipyramid trigonal copper(II) superoxido complexes are analyzed by using theoretical approaches based on wavefunction methods. We present a detailed study on the $[(\text{tren})\text{Cu}(\text{O}_2)]^+$ complex, which shares similar features with the $[(\text{TMG}_3\text{tren})\text{Cu}(\text{O}_2)]^+$ and $[(\text{TMPA})\text{Cu}(\text{O}_2)]^+$ systems.

Concerning the absorption spectrum of the complexes, our study based on multireference methods allows us to understand that the IL transition leads to the dark state T1 (first excited triplet state). Previously, it has been proposed that this IL transition would lie in between the $d-d$ bands. However, in this re-

gion of the spectrum, several states are found that imply not only the $d-d$ transitions, but also doubly excited states with respect to the $|ROHF\rangle$ configuration. These states result either from combined MLCT and LMCT transitions, or from simultaneous IL and $d-d$ transitions and they do not imply a significant net charge transfer. Our study suggests that band 3, previously assigned to the IL, has not a pure IL character, but must correspond to a doubly excited state. The LMCT band follows at higher energy, as expected.

Within TD-DFT and TDA approaches, the doubly excited states can not be recovered, but the IL and the $d-d$ transitions are eventually well reproduced, see TD-DFT values in Table 1 and in the Supporting Information. The energy of the LMCT band is also reasonably accurate, notably within the TDA approach, see Table 3.

Multireference methods are useful to understand the nature of the ground and excited states of this family of mixed-valence complexes, lying between Cu^{II} and Cu^{I}. For this class of complexes, we reach the limits of applicability of CASSCF-CASPT2 methods with currently available computing resources. We highlight the usefulness of approximate CI schemes such as ICE-CI or DMRG, in combination with the RASSCF-RASPT2 approach, to account for a significant part of the electronic correlation at play. The analysis of ground and excited states has implications for catalysis as these complexes can be involved in multi-state reactivity or photo-chemical processes.

Acknowledgement The authors thank the French Research Ministry, Aix-Marseille University and CNRS for financial support. Centre de Calcul Intensif d'Aix-Marseille is acknowledged for granting access to its high performance computing resources (project b288). We also thank Huanchen Zhai for his help setting up DMRG calculation with BLOCK2 and Felix Plasser for his support with the libWFA library. Finally, we are thankful to Emmanuel Giner for useful discussion on the subject.

Supporting Information Available

Supporting Information: selected active spaces, results for $[(NH_3)Cu(O_2)]^+$ and $[(TMPA)Cu(O_2)]^+$, density plots, CSFs' weights and their schematic representations, results with enlarged active spaces, DMRG-NEVPT2 and TD-DFT results, complete state analysis using 1-TDM and the ICE-CI method, analysis of distortion parameters, geometrical parameters. (PDF).

References

(1) Solomon, E. I.; Heppner, D. E.; Johnston, E. M.; Ginsbach, J. W.; Cirera, J.; Qayyum, M.; Kieber-Emmons, M. T.; Kjaergaard, C. H.; Hadt, R. G.; Tian, L. Copper Active Sites in Biology. *Chem. Rev.* **2014**, *114*, 3659–3853.

(2) Chen, P.; Solomon, E. I. O_2 activation by binuclear Cu sites: Noncoupled versus exchange coupled reaction mechanisms. *Proc. Natl. Acad. Sci.* **2004**, *101*, 13105–13110.

(3) Solomon, E. I.; Ginsbach, J. W.; Heppner, D. E.; Kieber-Emmons, M. T.; Kjaergaard, C. H.; Smeets, P. J.; Tian, L.; Woertink, J. S. Copper Dioxygen (Bio)Inorganic Chemistry. *Faraday Discuss.* **2011**, *148*, 11–108.

(4) Peterson, R. L.; Ginsbach, J. W.; Cowley, R. E.; Qayyum, M. F.; Himes, R. A.; Siegler, M. A.; Moore, C. D.; Hedman, B.; Hodgson, K. O.; Fukuzumi, S.; Solomon, E. I.; Karlin, K. D. Stepwise Protonation and Electron-Transfer Reduction of a Primary Copper–Dioxygen Adduct. *J. Am. Chem. Soc.* **2013**, *135*, 16454–16467.

(5) Liu, J. J.; Diaz, D. E.; Quist, D. A.; Karlin, K. D. Copper(I)-Dioxygen Adducts and Copper Enzyme Mechanisms. *Isr. J. Chem.* **2016**, *56*, 738–755.

(6) Elwell, C. E.; Gagnon, N. L.; Neisen, B. D.; Dhar, D.; Spaeth, A. D.; Yee, G. M.; Tolman, W. B. Copper–Oxygen Complexes Revisited: Structures, Spectroscopy, and Reactivity. *Chem. Rev.* **2017**, *117*, 2059–2107.

(7) De Leener, G.; Over, D.; Smet, C.; Cornut, D.; Porras-Gutierrez, A. G.; López, I.; Douziech, B.; Le Poul, N.; Topić, F.; Rissanen, K.; Le Mest, Y.; Jabin, I.; Reinaud, O. "Two-Story" Calix[6]arene-Based Zinc and Copper Complexes: Structure, Properties, and O_2 Binding. *Inorg. Chem.* **2017**, *56*, 10971–10983.

(8) Diaz, D. E.; Quist, D. A.; Herzog, A. E.; Schaefer, A. W.; Kipouros, I.; Bhadra, M.; Solomon, E. I.; Karlin, K. D. Impact of Intramolecular Hydrogen Bonding on the Reactivity of Cupric Superoxide Complexes with OH and CH Substrates. *Angew. Chem. Int. Ed.* **2019**, *58*, 17572–17576.

(9) Ehudin, M. A.; Schaefer, A. W.; Adam, S. M.; Quist, D. A.; Diaz, D. E.; Tang, J. A.; Solomon, E. I.; Karlin, K. D. Influence of intramolecular secondary sphere hydrogen-bonding interactions on cytochrome c oxidase inspired low-spin heme–peroxo–copper complexes. *Chem. Sci.* **2019**, *10*, 2893–2905.

(10) Kim, B.; Karlin, K. D. Ligand–Copper(I) Primary O_2-Adducts: Design, Characterization, and Biological Significance of Cupric–Superoxides. *Acc. Chem. Res.* **2023**, *56*, 2197–2212.

(11) Fujisawa, K.; Tanaka, M.; Moro-oka, Y.; Kitajima, N. A Monomeric Side-On Superoxocopper(II) Complex: $Cu(O_2)(HB(3\text{-}tBu\text{-}5\text{-}iPrpz)_3)$. *J. Am. Chem. Soc.* **1994**, *116*, 12079–12080.

(12) Chen, P.; Root, D. E.; Campochiaro, C.; Fujisawa, K.; Solomon, E. I. Spectroscopic and Electronic Structure Studies of the Diamagnetic Side-On Cu(II)-Superoxo Complex $Cu(O_2)[HB(3\text{-}R\text{-}5\text{-}^{i}Prpz)_3]$: Antiferromagnetic Coupling versus Covalent Delocalization. *J. Am. Chem. Soc.* **2003**, *125*, 466–474.

(13) Cramer, C. J.; Gour, J. R.; Kinal, A.; Włoch, M.; Piecuch, P.; Moughal Shahi, A. R.; Gagliardi, L. Stereoelectronic Effects on Molecular Geometries and State-Energy Splittings of Ligated Monocopper Dioxygen Complexes. *J. Phys. Chem. A* **2008**, *112*, 3754–3767.

(14) Schatz, M.; Raab, V.; Foxon, S. P.; Brehm, G.; Schneider, S.; Reiher, M.; Holthausen, M. C.; Sundermeyer, J.; Schindler, S. Combined Spectroscopic and Theoretical Evidence for a Persistent End-On Copper Superoxo Complex. *Angew Chem Int Ed* **2004**, *43*, 4360–4363.

(15) Würtele, C.; Gaoutchenova, E.; Harms, K.; Holthausen, M. C.; Sundermeyer, J.; Schindler, S. Crystallographic Characterization of a Synthetic 1:1 End-On Copper Dioxygen Adduct Complex. *Angew Chem Int Ed* **2006**, *45*, 3867–3869.

(16) Ginsbach, J. W.; Peterson, R. L.; Cowley, R. E.; Karlin, K. D.; Solomon, E. I. Correlation of the Electronic and Geometric Structures in Mononuclear Copper(II) Superoxide Complexes. *Inorg. Chem.* **2013**, 12872–12874.

(17) Weitzer, M.; Schindler, S.; Brehm, G.; Schneider, S.; Hörmann, E.; Jung, B.; Kaderli, S.; Zuberbühler, A. D. Reversible Binding of Dioxygen by the Copper(I) Complex with Tris(2-dimethylaminoethyl)amine (Me_6tren) Ligand. *Inorg. Chem.* **2003**, *42*, 1800–1806.

(18) Komiyama, K.; Furutachi, H.; Nagatomo, S.; Hashimoto, A.; Hayashi, H.; Fujinami, S.; Suzuki, M.; Kitagawa, T. Dioxygen Reactivity of Copper(I) Complexes with Tetradentate Tripodal Ligands Having Aliphatic Nitrogen Donors:

Synthesis, Structures, and Properties of Peroxo and Superoxo Complexes. *Bull. Chem. Soc. Jpn.* **2004**, *77*, 59–72.

(19) Woertink, J. S.; Tian, L.; Maiti, D.; Lucas, H. R.; Himes, R. A.; Karlin, K. D.; Neese, F.; Würtele, C.; Holthausen, M. C.; Bill, E.; Sundermeyer, J.; Schindler, S.; Solomon, E. I. Spectroscopic and Computational Studies of an End-on Bound Superoxo-Cu(II) Complex: Geometric and Electronic Factors That Determine the Ground State. *Inorg. Chem.* **2010**, *49*, 9450–9459.

(20) Kobayashi, Y.; Ohkubo, K.; Nomura, T.; Kubo, M.; Fujieda, N.; Sugimoto, H.; Fukuzumi, S.; Goto, K.; Ogura, T.; Itoh, S. Copper(I)-Dioxygen Reactivity in a Sterically Demanding Tripodal Tetradentate tren Ligand: Formation and Reactivity of a Mononuclear Copper(II) End-On Superoxo Complex. *Eur. J. Inorg. Chem.* **2012**, *2012*, 4574–4578.

(21) Bhadra, M.; Lee, J. Y. C.; Cowley, R. E.; Kim, S.; Siegler, M. A.; Solomon, E. I.; Karlin, K. D. Intramolecular Hydrogen Bonding Enhances Stability and Reactivity of Mononuclear Cupric Superoxide Complexes. *J. Am. Chem. Soc.* **2018**, *140*, 9042–9045.

(22) Will, J.; Würtele, C.; Becker, J.; Walter, O.; Schindler, S. Synthesis, crystal structures and reactivity towards dioxygen of copper(I) complexes with tripodal aliphatic amine ligands. *Polyhedron* **2019**, *171*, 448–454.

(23) Quek, S. Y.; Debnath, S.; Laxmi, S.; van Gastel, M.; Krämer, T.; England, J. Sterically Stabilized End-On Superoxocopper(II) Complexes and Mechanistic Insights into Their Reactivity with O–H, N–H, and C–H Substrates. *J. Am. Chem. Soc.* **2021**, *143*, 19731–19747.

(24) Maitra, N. T. Double and Charge-Transfer Excitations in Time-Dependent Density Functional Theory. *Annu. Rev. Phys. Chem.* **2022**, *73*, 117–140.

(25) Malmqvist, P. Å.; Pierloot, K.; Shahi, A. R. M.; Cramer, C. J.; Gagliardi, L. The Restricted Active Space Followed by Second-Order Perturbation Theory Method: Theory and Application to the Study of CuO_2 and Cu_2O_2 Systems. *J. Chem. Phys.* **2008**, *128*, 204109.

(26) Giner, E.; Tew, D. P.; Garniron, Y.; Alavi, A. Interplay between Electronic Correlation and Metal–Ligand Delocalization in the Spectroscopy of Transition Metal Compounds: Case Study on a Series of Planar Cu^{2+} Complexes. *J. Chem. Theory Comput.* **2018**, *14*, 6240–6252.

(27) Varela Lambraño, R.; Vivas-Reyes, R.; Visbal, R.; Zapata-Rivera, J. Evaluation of the electronic structure and charge transfer in the $(Cu_2O_2)^{2+}$ core using multiconfigurational methods. *Theor Chem Acc* **2020**, *139*, 56.

(28) Cramer, C. J.; Włoch, M.; Piecuch, P.; Puzzarini, C.; Gagliardi, L. Theoretical Models on the Cu_2O_2 Torture Track: Mechanistic Implications for Oxytyrosinase and Small-Molecule Analogues. *J. Phys. Chem. A* **2006**, *110*, 1991–2004.

(29) Cramer, C. J.; Kinal, A.; Włoch, M.; Piecuch, P.; Gagliardi, L. Theoretical Characterization of End-On and Side-On Peroxide Coordination in Ligated Cu_2O_2 Models. *J. Phys. Chem. A* **2006**, *110*, 11557–11568.

(30) Zhai, H.; Chan, G. K.-L. Low Communication High Performance Ab Initio Density Matrix Renormalization Group Algorithms. *J. Chem. Phys.* **2021**, *154*, 224116.

(31) Chilkuri, V. G.; Neese, F. Comparison of Many-Particle Representations for Selected Configuration Interaction: II. Numerical Benchmark Calculations. *J. Chem. Theory Comput.* **2021**, *17*, 2868–2885.

(32) Chilkuri, V. G.; Neese, F. Comparison of Many-particle Representations for selected-CI I: A Tree Based Approach. *J. Comput. Chem.* **2021**, *42*, 982–1005.

(33) Guo, Y.; Sivalingam, K.; Neese, F. Approximations of Density Matrices in N-electron Valence State Second-Order Perturbation Theory (NEVPT2). I. Revisiting the NEVPT2 Construction. *J. Chem. Phys.* **2021**, *154*, 214111.

(34) Guo, Y.; Sivalingam, K.; Kollmar, C.; Neese, F. Approximations of Density Matrices in N-electron Valence State Second-Order Perturbation Theory (NEVPT2). II. The Full Rank NEVPT2 (FR-NEVPT2) Formulation. *J. Chem. Phys.* **2021**, *154*, 214113.

(35) Fdez. Galván, I. et al. OpenMolcas: From Source Code to Insight. *J. Chem. Theory Comput.* **2019**, *15*, 5925–5964.

(36) Aquilante, F. et al. Modern Quantum Chemistry with [Open]Molcas. *J. Chem. Phys.* **2020**, *152*, 214117.

(37) Plasser, F. TheoDORE: A Toolbox for a Detailed and Automated Analysis of Electronic Excited State Computations. *J. Chem. Phys.* **2020**, *152*, 084108.

(38) Mai, S.; Plasser, F.; Dorn, J.; Fumanal, M.; Daniel, C.; González, L. Quantitative Wave Function Analysis for Excited States of Transition Metal Complexes. *Coord. Chem. Rev.* **2018**, *361*, 74–97.

(39) TURBOMOLE V7.5 2020, a Development of University of Karlsruhe and Forschungszentrum Karlsruhe GmbH, 1989-2007, TURBOMOLE GmbH, since 2007; Available from https://www.turbomole.org.

(40) Dirac, P. A. M.; Fowler, R. H. Quantum Mechanics of Many-Electron Systems. *Proc. Royal Soc. (London)* **1929**, *123*, 714–733.

(41) Slater, J. C. A Simplification of the Hartree-Fock Method. *Phys. Rev.* **1951**, *81*, 385–390.

(42) Perdew, J. P.; Wang, Y. Accurate and Simple Analytic Representation of the Electron-Gas Correlation Energy. *Phys. Rev. B* **1992**, *45*, 13244–13249.

(43) Perdew, J. P.; Burke, K.; Ernzerhof, M. Generalized Gradient Approximation Made Simple. *Phys. Rev. Lett.* **1996**, *77*, 3865–3868.

(44) Perdew, J. P.; Ernzerhof, M.; Burke, K. Rationale for Mixing Exact Exchange with Density Functional Approximations. *J. Chem. Phys.* **1996**, *105*, 9982–9985.

(45) Weigend, F.; Furche, F.; Ahlrichs, R. Gaussian Basis Sets of Quadruple Zeta Valence Quality for Atoms H–Kr. *J. Chem. Phys.* **2003**, *119*, 12753–12762.

(46) Weigend, F.; Ahlrichs, R. Balanced Basis Sets of Split Valence, Triple Zeta Valence and Quadruple Zeta Valence Quality for H to Rn: Design and Assessment of Accuracy. *Phys. Chem. Chem. Phys.* **2005**, *7*, 3297–3305.

(47) Eichkorn, K.; Treutler, O.; Öhm, H.; Häser, M.; Ahlrichs, R. Auxiliary Basis Sets to Approximate Coulomb Potentials. *Chem. Phys. Lett.* **1995**, *240*, 283–290.

(48) Eichkorn, K.; Weigend, F.; Treutler, O.; Ahlrichs, R. Auxiliary Basis Sets for Main Row Atoms and Transition Metals and Their Use to Approximate Coulomb Potentials. *Theor Chem Acta* **1997**, *97*, 119–124.

(49) Weigend, F. Accurate Coulomb-fitting Basis Sets for H to Rn. *Phys. Chem. Chem. Phys.* **2006**, *8*, 1057–1065.

(50) Aquilante, F.; Malmqvist, P.-Å.; Pedersen, T. B.; Ghosh, A.; Roos, B. O. Cholesky Decomposition-Based Multiconfiguration Second-Order Perturbation

Theory (CD-CASPT2): Application to the Spin-State Energetics of CoIII(Diiminato)(NPh). *J. Chem. Theory Comput.* **2008**, *4*, 694–702.

(51) Aquilante, F.; Gagliardi, L.; Pedersen, T. B.; Lindh, R. Atomic Cholesky Decompositions: A Route to Unbiased Auxiliary Basis Sets for Density Fitting Approximation with Tunable Accuracy and Efficiency. *J. Chem. Phys.* **2009**, *130*, 154107.

(52) Ghigo, G.; Roos, B. O.; Malmqvist, P.-Å. A Modified Definition of the Zeroth-Order Hamiltonian in Multiconfigurational Perturbation Theory (CASPT2). *Chem. Phys. Lett.* **2004**, *396*, 142–149.

(53) Forsberg, N.; Malmqvist, P.-Å. Multiconfiguration Perturbation Theory with Imaginary Level Shift. *Chem. Phys. Lett.* **1997**, *274*, 196–204.

(54) Sun, Q.; Berkelbach, T. C.; Blunt, N. S.; Booth, G. H.; Guo, S.; Li, Z.; Liu, J.; McClain, J. D.; Sayfutyarova, E. R.; Sharma, S.; Wouters, S.; Chan, G. K.-L. P Y SCF: The Python-based Simulations of Chemistry Framework. *WIREs Comput Mol Sci* **2018**, *8*.

(55) Stoychev, G. L.; Auer, A. A.; Neese, F. Automatic Generation of Auxiliary Basis Sets. *J. Chem. Theory Comput.* **2017**, *13*, 554–562.

(56) Roemelt, M.; Guo, S.; Chan, G. K.-L. A projected approximation to strongly contracted N-electron valence perturbation theory for DMRG wavefunctions. *J. Chem. Phys.* **2016**, *144*, 204113.

(57) Sokolov, A. Y.; Guo, S.; Ronca, E.; Chan, G. K.-L. Time-Dependent N-electron Valence Perturbation Theory with Matrix Product State Reference Wavefunctions for Large Active Spaces and Basis Sets: Applications to the Chromium Dimer and All-Trans Polyenes. *J. Chem. Phys.* **2017**, *146*, 244102.

(58) Zobel, J. P.; Widmark, P.-O.; Veryazov, V. The ANO-R Basis Set. *J. Chem. Theory Comput.* **2020**, *16*, 278–294.

(59) Sikkema, J.; Visscher, L.; Saue, T.; Iliaš, M. The Molecular Mean-Field Approach for Correlated Relativistic Calculations. *J. Chem. Phys.* **2009**, *131*, 124116.

(60) Neese, F. Software Update: The ORCA Program System—Version 5.0. *WIREs Comput. Mol. Sci.* **2022**, *12*, e1606.

(61) Plasser, F.; Krylov, A. I.; Dreuw, A. Libwfa: Wavefunction Analysis Tools for Excited and Open-shell Electronic States. *WIREs Comput Mol Sci* **2022**, *12*.

(62) Andersson, K.; Roos, B. O. Excitation Energies in the Nickel Atom Studied with the Complete Active Space SCF Method and Second-Order Perturbation Theory. *Chem. Phys. Lett.* **1992**, *191*, 507–514.

(63) Pierloot, K. Transition Metals Compounds: Outstanding Challenges for Multiconfigurational Methods. *Int. J. Quantum Chem.* **2011**, *111*, 3291–3301.

(64) Sauri, V.; Serrano-Andrés, L.; Shahi, A. R. M.; Gagliardi, L.; Vancoillie, S.; Pierloot, K. Multiconfigurational Second-Order Perturbation Theory Restricted Active Space (RASPT2) Method for Electronic Excited States: A Benchmark Study. *J. Chem. Theory Comput.* **2011**, *7*, 153–168.

(65) Gagliardi, L.; Lindh, R.; Karlström, G. Local Properties of Quantum Chemical Systems: The LoProp Approach. *J. Chem. Phys.* **2004**, *121*, 4494–4500.

(66) Giner, E.; Angeli, C. Metal-Ligand Delocalization and Spin Density in the $CuCl_2$ and $[CuCl_4]^{2-}$ Molecules: Some Insights from Wave Function Theory. *J. Chem. Phys.* **2015**, *143*, 124305.

(67) Li Manni, G.; Alavi, A. Understanding the Mechanism Stabilizing Intermediate Spin States in Fe(II)-Porphyrin. *J. Phys. Chem. A* **2018**, *122*, 4935–4947.

(68) Hiberty, P. C.; Humbel, S.; Byrman, C. P.; van Lenthe, J. H. Compact Valence Bond Functions with Breathing Orbitals: Application to the Bond Dissociation Energies of F2 and FH. *J. Chem. Phys.* **1994**, *101*, 5969–5976.

(69) Hiberty, P. C.; Shaik, S. Breathing-Orbital Valence Bond Method – a Modern Valence Bond Method That Includes Dynamic Correlation. *Theor. Chem. Acc.* **2002**, *108*, 255–272.

(70) Barca, G. M. J.; Gilbert, A. T. B.; Gill, P. M. W. Excitation Number: Characterizing Multiply Excited States. *J. Chem. Theory Comput.* **2018**, *14*, 9–13.

(71) Ravi, M.; Choon Park, Y.; Perera, A.; Bartlett, R. J. The Intermediate State Approach for Doubly Excited Dark States in EOM-coupled-cluster Theory. *J. Chem. Phys.* **2022**, *156*, 201102.

TOC Graphic

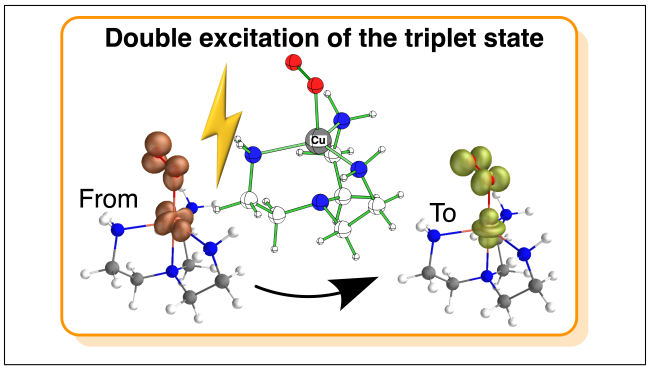

Doubly excited states in the $d - d$ region of the absorption spectrum of bipyramid trigonal copper(II) superoxido complexes are unveiled by employing multireference methods.